

# Chiral three-nucleon forces for the new local position-space two-nucleon potential in *ab initio* many-body calculations

R. Z. Hu <sup>a</sup>, J. G. Li <sup>b,c</sup>, S. Q. Fan <sup>a</sup>, F. R. Xu <sup>a,b,c,\*</sup>

<sup>a</sup>*School of Physics, and State Key Laboratory of Nuclear Physics and Technology, Peking University, Beijing 100871, China*

<sup>b</sup>*Institute of Modern Physics, Chinese Academy of Sciences, Lanzhou 730000, China*

<sup>c</sup>*Southern Center for Nuclear-Science Theory, Institute of Modern Physics, Chinese Academy of Sciences, Huizhou 516000, China*

<sup>d</sup>*School of Nuclear Science and Technology, University of Chinese Academy of Sciences, Beijing 100049, China*

## Abstract

Three-nucleon force (3NF) plays an important role in understanding the structure of finite nuclei and the saturation properties of infinite nuclear matter. The chiral 3NF derived from the chiral effective field theory has been successful in *ab initio* studies of atomic nuclei. However, challenges remain, such as parameterizing low-energy constants and applying regulators. Most of established chiral nuclear forces have a nonlocal form in the momentum space. In this work, we construct local and hybrid local-nonlocal chiral 3NFs for the newly established Idaho local position-space two-nucleon potential, and calculate binding energies and radii of nuclei up to  $^{132}\text{Sn}$ . The two low-energy constants of 3NF are constrained by the ground-state energies of  $^3\text{H}$  and  $^{16}\text{O}$ , as suggested in a recent work. The chiral Hamiltonian obtained with the local-nonlocal regulator can simultaneously reproduce the experimental ground-state energies and charge radii of nuclei over a large range from  $^4\text{He}$  to  $^{132}\text{Sn}$ .

**Keywords:** Three-nucleon forces; Low-energy constants; Binding energy; Charge radius

## 1. Introduction

One of the main goals of *ab initio* nuclear theory is to understand atomic nuclei and nuclear matter from the fundamental degrees of freedom and interactions [1, 2]. Within the framework of the chiral effective field theory ( $\chi$ EFT), two-nucleon and three-nucleon forces (2NF and 3NF, respectively) naturally emerge at different orders arranged by a proper power counting scheme [3, 4]. At a given chiral order, chiral nucleon interactions are renormalized by multiplying regulator functions that suppress high-momentum contributions beyond a certain cut-off momentum [5, 6]. Low-energy constants (LECs) appearing in chiral interactions are determined by available experimental data [7, 8]. Chiral Hamiltonians obtained thus have been successfully applied to *ab initio* calculations of strongly correlated many-body nuclei and nuclear matter [9–15].

Nevertheless, open questions still remain for  $\chi$ EFT-based nuclear forces. One of the most important questions is whether the chiral interaction can simultaneously reproduce experimental ground-state energies and charge radii of medium-mass nuclei, and the saturation properties of nuclear matter [16, 17]. Though many efforts have been made to address this issue by including many-body observables in the determination of 3NF LECs or by introducing different regularization schemes [18–21], the situation is still unclear, and further investigations are needed [22, 23].

Most of previous nuclear *ab initio* calculations were based on nonlocal momentum-space potentials. Local position-space

potentials were explored mainly for light-mass nuclei ( $A \lesssim 16$ ) using quantum Monte Carlo (QMC) methods [24, 25]. However, the situation for heavier nuclei is barely known due to the computation limits of QMC methods. In this work, we construct a chiral 3NF for the new position-space 2NF developed by the Idaho group [26]. The new family of chiral 2NF plus 3NF with a proper local-nonlocal regularization scheme can provide promising *ab initio* many-body calculations of nuclear structure.

## 2. Chiral three-nucleon forces and regulators

The  $A$ -body intrinsic Hamiltonian can be written as

$$\hat{H} = \frac{1}{A} \sum_{i < j}^A \frac{(p_i - p_j)^2}{2m} + \sum_{i < j}^A \hat{V}_{\text{NN}}^{ij} + \sum_{i < j < k}^A \hat{V}_{\text{3N}}^{ijk}, \quad (1)$$

where the first term denotes the intrinsic kinetic energy, whereas  $\hat{V}_{\text{NN}}$  and  $\hat{V}_{\text{3N}}$  indicate 2NF and 3NF, respectively. In the present work, to improve many-body calculations, we want to construct a chiral 3NF which complements the chiral local position-space 2NF developed recently by the Idaho group [26]. The local position-space 2NF was obtained by the chiral expansion up to the  $N^3\text{LO}$  with a position-space regulator cutoff  $R_\pi = 1.2 \text{ fm}$  [26]. To seed up the convergences of many-body calculations of medium-mass nuclei, the 2NF is evolved to a low-momentum scale  $\lambda = 2.2 \text{ fm}^{-1}$  using the similarity renormalization group (SRG) [27, 28]. The resulting low-resolution 2NF has been successfully applied to *ab initio* no-core shell model (NCSM) calculations of low-lying states and electromagnetic properties of  $^{10}\text{B}$  [29, 30]. We have checked that the

\*frxu@pku.edu.cn

$\lambda$  dependence of the results can be largely absorbed by adjusting the 3NF LECs, which equivalently considers induced-3NF effects.

The chiral 3NF at N<sup>2</sup>LO consists of three topologies [31, 32],

$$\hat{V}_{3N} = \hat{V}_{3N}^{2\pi} + \hat{V}_{3N}^{1\pi} + \hat{V}_{3N}^{ct}. \quad (2)$$

The long-range two- $\pi$  exchange term  $\hat{V}_{3N}^{2\pi}$  contains three pion-nucleon ( $\pi N$ ) scattering LECs which take  $c_1 = -0.74 \text{ GeV}^{-1}$ ,  $c_3 = -3.61 \text{ GeV}^{-1}$  and  $c_4 = 2.44 \text{ GeV}^{-1}$  [26, 33, 34] determined by the Roy-Steiner-equation scattering analysis at N<sup>2</sup>LO [33, 35]. The intermediate-range one-pion exchange  $\hat{V}_{3N}^{1\pi}$  and short-range three-nucleon contact term  $\hat{V}_{3N}^{ct}$  contain two additional LECs,  $c_D$  and  $c_E$ , respectively.

Similar to the 2NF, the chiral 3NF also needs to be applied with regulator functions to suppress high-momentum contributions. Several forms of the regulator function have been proposed, including the local form [36]

$$f_{\text{local}} = \exp \left[ - \left( \frac{|p'_2 - p_2|^2}{\Lambda^2} \right)^2 - \left( \frac{|p'_3 - p_3|^2}{\Lambda^2} \right)^2 \right], \quad (3)$$

the nonlocal form [32]

$$f_{\text{nonlocal}} = \exp \left[ - \left( \frac{4p^2 + 3q^2}{4\Lambda'^2} \right)^2 - \left( \frac{4p'^2 + 3q'^2}{4\Lambda'^2} \right)^2 \right], \quad (4)$$

and the hybrid local-nonlocal (lnl) form [21]

$$f_{\text{lnl}} = f_{\text{local}} f_{\text{nonlocal}}, \quad (5)$$

with  $p_i$  ( $p'_i$ ) being the initial (final) momentum of  $i$ th nucleon,  $p$  and  $q$  ( $p'$  and  $q'$ ) being the magnitude of initial (final) Jacobi momenta.  $\Lambda$  ( $\Lambda'$ ) is the  $\chi$ EFT hard cutoff. We have tested the two different regularization schemes to see the difference. The cutoffs are set to be  $\Lambda = 500 \text{ MeV}$  for the local regulator, and  $\Lambda = 700 \text{ MeV}$  and  $\Lambda' = 500 \text{ MeV}$  for the lnl regulator. Other different cutoffs of  $\Lambda$  ( $\Lambda'$ ) have also been tested, obtaining similar results without conclusions changed.

### 3. Parameterization of LECs $c_D$ and $c_E$ of chiral three-nucleon force

There is still no unified agreement on strategies to constrain the 3NF LECs  $c_D$  and  $c_E$  [18, 20, 34, 36]. However, at least two uncorrelated observables are required to determine  $c_D$  and  $c_E$  values. In this work, we use the  $^3\text{H}$  ground-state energy  $E(^3\text{H})$  as the first constraint on  $c_D$  and  $c_E$ . Though there have been attempts to use the binding energy or charge radius of  $^4\text{He}$  as the second constraint [37, 38], in many cases this strategy does not seem to be a good choice [20], primarily due to the strong correlation between these observables [39]. In Ref. [20], it was suggested to use the  $^{16}\text{O}$  ground-state energy  $E(^{16}\text{O})$  as the second constraint, which we follow in the present work.

The  $^3\text{H}$  energy is calculated using the NCSM in the Jacobi coordinates [40]. The calculation is converged at a harmonic oscillator (HO) frequency around  $\hbar\Omega = 24 \text{ MeV}$  with

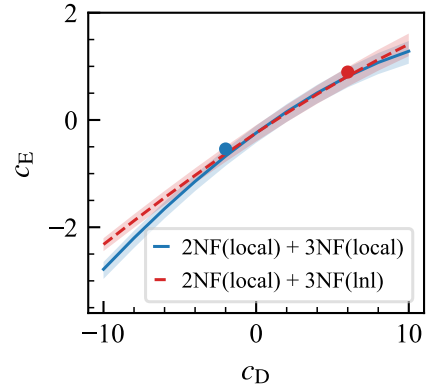


Figure 1: Relation between  $c_D$  and  $c_E$  obtained by the constraint of the  $^3\text{H}$  binding energy, for the local and lnl 3NF regulators. Shadows indicate the EFT uncertainty of 300 keV. The blue and red filled dots are the final optimized results by considering the  $^{16}\text{O}$  binding energy for 2NF(local)+3NF(local) and 2NF(local)+3NF(lnl), respectively.

$N_{\text{max}} = 44$  HO shells. The  $^3\text{H}$  NCSM calculation with such large model space should be considered to be exact, and the many-body uncertainty should be ignored. The dominant uncertainty should be from the  $\chi$ EFT truncation. Uncertainties caused by  $\chi$ EFT can be estimated, e.g., for an observable  $X$  at N<sup>2</sup>LO and N<sup>3</sup>LO, via [41–43]

$$\Delta X_{\text{N}^2\text{LO}} = \max \left( Q^4 |X_{\text{LO}}|, Q^2 |X_{\text{LO}} - X_{\text{NLO}}|, Q |X_{\text{NLO}} - X_{\text{N}^2\text{LO}}| \right), \quad (6)$$

and

$$\Delta X_{\text{N}^3\text{LO}} = \max \left( Q^5 |X_{\text{LO}}|, Q^3 |X_{\text{LO}} - X_{\text{NLO}}|, Q^2 |X_{\text{NLO}} - X_{\text{N}^2\text{LO}}|, Q |X_{\text{N}^2\text{LO}} - X_{\text{N}^3\text{LO}}| \right), \quad (7)$$

respectively, where  $Q$  is the EFT expansion scale measured by the ratio of the nucleon momentum transfer over the EFT hard cutoff  $\Lambda$ , which can be estimated by the pion mass over  $\Lambda$ . For  $\Lambda \sim 600 \text{ MeV}$ , the typical value is  $Q \sim 1/3$  [20, 39] which is used in quantifying the EFT uncertainty. We have estimated that uncertainties from the  $\chi$ EFT truncation at N<sup>2</sup>LO and N<sup>3</sup>LO are 446 keV and 149 keV, respectively, for the  $^3\text{H}$  ground-state energy. This means that, in optimizing the 3NF LECs  $c_D$  and  $c_E$ , we should endure an uncertainty of approximately 300 keV for the  $^3\text{H}$  ground-state energy. The constraint by the  $^3\text{H}$  binding energy results in a relation between  $c_D$  and  $c_E$ , as shown in Fig. 1.

As suggested in Ref. [20], the  $^{16}\text{O}$  ground-state energy is used as a constraint to fix the values of  $c_D$  and  $c_E$ . We use the IMSSRG in the Magnus formulation [44, 45] to calculate the  $^{16}\text{O}$  ground-state energy. The many-body Hamiltonian is normal ordered with respect to the reference state of the Hartree-

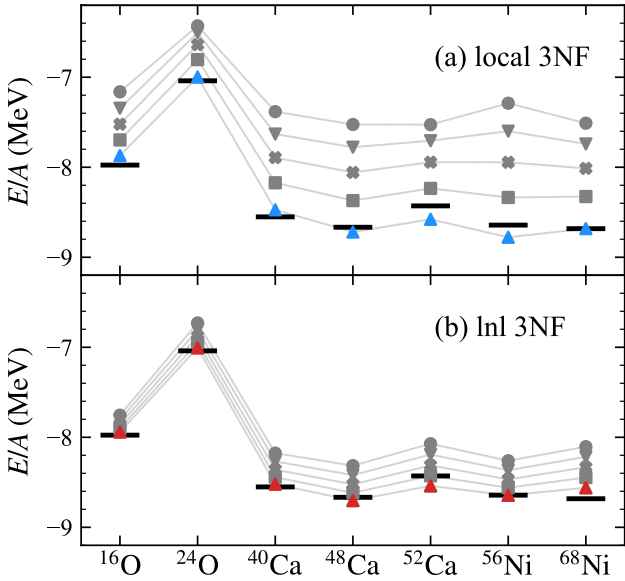


Figure 2: Ground-state energies of selected medium-mass doubly-closed-shell nuclei, calculated by IMSRG with increasing the  $c_D$  value in a step of 1.0, starting from  $c_D = -6.0$  for the local 3NF regulator (a), and from  $c_D = 2.0$  for the lnl regulator (b). The black bars indicate experimental data [48].

Fock ground state as [46, 47]

$$\hat{H} = E_0 + \sum_{ij} f_{ij} \{ \hat{a}_i^\dagger \hat{a}_j \} + \frac{1}{2!^2} \sum_{ijkl} \Gamma_{ijkl} \{ \hat{a}_i^\dagger \hat{a}_j^\dagger \hat{a}_k \hat{a}_l \} + \frac{1}{3!^2} \sum_{ijklmn} W_{ijklmn} \{ \hat{a}_i^\dagger \hat{a}_j^\dagger \hat{a}_k^\dagger \hat{a}_m \hat{a}_n \hat{a}_l \}, \quad (8)$$

where  $E_0$ ,  $f$ ,  $\Gamma$  and  $W$  represent normal-ordered zero-, one-, two- and three-body terms, respectively. In the IMSRG evolution, operators are truncated at the two-body level. It has been estimated that the total many-body uncertainty from the IMSRG evolution and normal-ordered approximation truncated at the two-body level is about 2% in energy calculations [20]. We have carefully calculated the ground-state energies of medium-mass nuclei at closed shells by gradually increasing the  $c_D$  value with  $c_E$  also changing according to the relation obtained by the  $E(^3\text{H})$  constraint. It is found that the calculated energies are monotonously lowered with increasing the  $c_D$  value. For the local 3NF regulator, calculations with  $c_D$  increasing starting from  $-6.0$  in a step of 1.0 show that  $c_D = -2.0$  gives good descriptions of experimental ground-state energies of the medium-mass closed-shell nuclei, as shown in the upper panel of Fig. 2. For the lnl 3NF regulator, calculations with  $c_D$  increasing starting from  $2.0$  in a step of 1.0 show that  $c_D = 6.0$  gives good descriptions of ground-state energies of the nuclei, see the lower panel of Fig. 2.

The optimal  $c_D$  and  $c_E$  values are summarized in Table 1 for the constructed 3NF with a local or lnl regulator. Note that we have only selected the integer values of  $c_D$  with a step of 1.0 in fitting, since errors (uncertainties) originating from IMSRG many-body and  $\chi$ EFT truncations are larger than the  $E(^{16}\text{O})$  change caused by a change of one unit in the  $c_D$  value. This

Table 1: Optimal  $c_D$  and  $c_E$  values, and calculated ground-state energies (in MeV) of  $^3\text{H}$  and  $^{16}\text{O}$ , compared with data [48]. The new local position-space Idaho potential [26] is used for the 2NF, while we construct a local or local-nonlocal (lnl) 3NF for this 2NF.

	$c_D$	$c_E$	$E(^3\text{H})$	$E(^{16}\text{O})$
3NF(local)	-2.0	-0.541	-8.78	-126.01
3NF(lnl)	6.0	0.894	-8.73	-127.15
Expt.			-8.482	-127.619

strategy is similar to that used in Ref. [20].

#### 4. Applications to the calculations of nuclear energies and radii

The constructed 3NF forms a family with the new local position-space 2NF proposed by the Idaho group [26]. We have used the new family of two- plus three-nucleon interactions to calculate the binding energies and charge radii of nuclei over a large range from  $^4\text{He}$  to  $^{132}\text{Sn}$ .

##### 4.1. Closed-shell nuclei

For closed-shell nuclei, the single-reference IMSRG can be used to calculate energies and radii of the ground states. The model space is restricted by the single-particle basis truncation  $e = 2n + l \leq e_{\max}$  and the 3NF matrix element truncation  $e_1 + e_2 + e_3 \leq E_{3\max}$ . In this work, we use  $e_{\max} = 14$  and  $E_{3\max} = 24$  [49] with optimized HO frequencies ( $\hbar\Omega$ ) to ensure model-space convergence in all cases.

We compare the present calculations with those obtained using some other well-established interactions, namely NN- $N^4\text{LO}^+$  [51] (with  $\Lambda = 500$  MeV), NN+3N(400) [21], NN+3N(lnl) [21], 1.8/2.0(EM) [38, 52, 53] and  $N^3\text{LO}(\text{H}\ddot{\text{u}}\text{t}\text{h})$  (both 2NF and 3NF at  $N^3\text{LO}$  with  $\Lambda = 500$  MeV) [20]. The results are shown in Fig. 3. We see that the present 2NF(local) plus 3NF(local) family describes binding energies well, but underestimates charge radii in general. If we use the hybrid 3NF regulator of locality and nonlocality defined as Eq. (5), the family of 2NF(local) plus 3NF(lnl) gives the most accurate descriptions of both binding energies and charge radii for the closed-shell nuclei from  $^4\text{He}$  to  $^{132}\text{Sn}$ , with deviations from experimental data below 2%, as shown in Fig. 3. The hybrid local-nonlocal 3NF regulator demonstrates its advantage in describing nuclear charge radii, which had also been indicated in previous studies [21].

##### 4.2. Open-shell nuclei

Open-shell nuclei can be calculated using the so-called valence-space IMSRG (VS-IMSRG) in which the valence-space effective Hamiltonian is obtained by the VS-IMSRG evolution [44]. Furthermore, to reduce the residual 3NF effect and choose a more appropriate shell-model core, the nucleus-dependent VS-IMSRG Hamiltonian with fractional filling of open-shell orbitals is used, named the ensemble normal ordering (ENO) [54]. The ENO VS-IMSRG evolution is also used

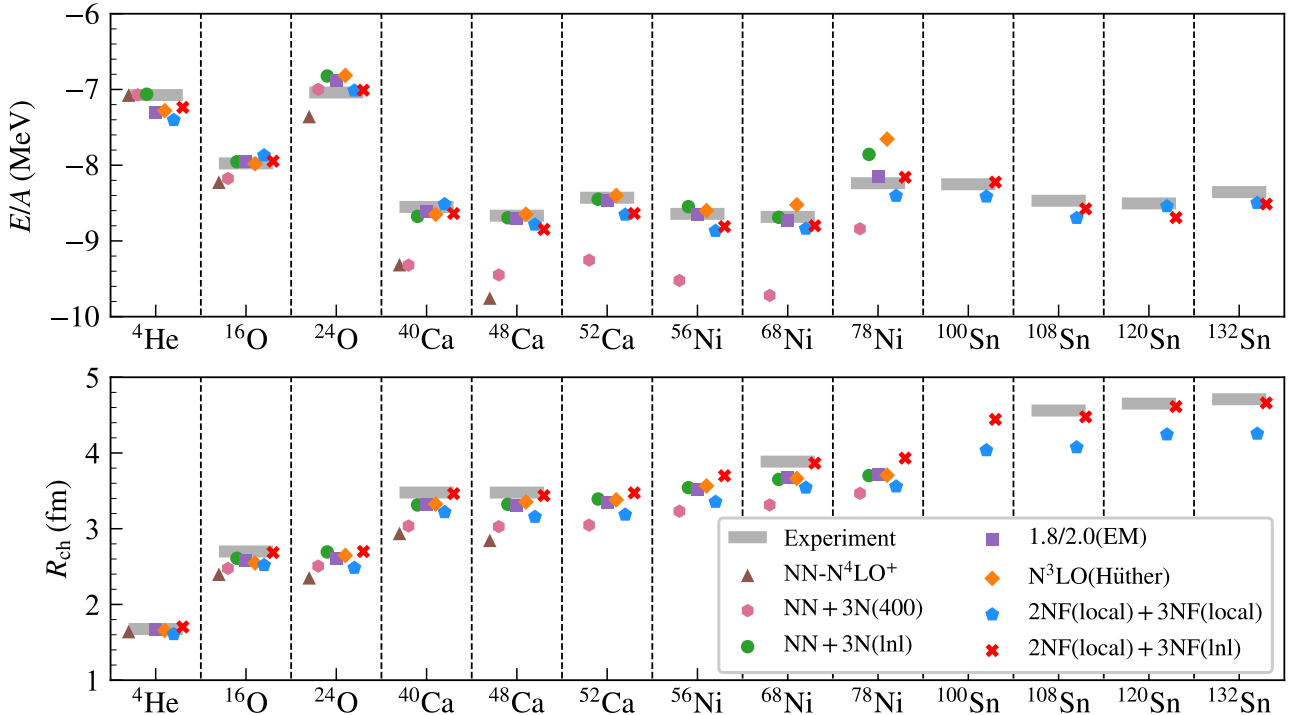


Figure 3: Ground-state energies per nucleon and charge radii for selected doubly-closed-shell nuclei from  $^4\text{He}$  to  $^{132}\text{Sn}$ . Experimental data are taken from Refs. [48, 50]. See text for details of the interactions and calculations.

to derive valence-space effective operators of other observables. The valence-space Hamiltonian is then diagonalized using the parallel shell model code `kshe11` [55]. In the present VS-IMSRG calculation, the valence space is defined as follows:  $p$  shell with  $^4\text{He}$  core for  $^{14}\text{O}$ ;  $sd$  shell with  $^{16}\text{O}$  core for  $^{17-28}\text{O}$ ,  $^{20-32}\text{Mg}$ ,  $^{22-34}\text{Si}$ ,  $^{28-36}\text{S}$ ,  $^{32-38}\text{Ar}$  and  $^{34-38}\text{Ca}$ ; proton  $sd$  and neutron  $pf$  shells with  $^{28}\text{O}$  core for  $^{34-40}\text{Mg}$ ,  $^{36-44}\text{Si}$ ,  $^{38-48}\text{S}$  and  $^{40-52}\text{Ar}$ ; and  $pf$  shell with  $^{40}\text{Ca}$  core for  $^{41-58}\text{Ca}$ .

Figure 4 shows the systematics of calculated ground-state energies, compared with experimental data, for oxygen, magnesium, silicon, sulfur, argon and calcium isotopic chains. We find that both local and lnl 3NFs give overall satisfying agreements with experimental ground-state energies for all isotopic chains investigated. Figure 5 shows charge radii for the isotopic chains studied. The situation is similar to closed-shell cases. The local-nonlocal 3NF connected to the new local position-space 2NF provides good descriptions of charge radii, while local 2NF with the same position-space 2NF underestimates the radii systematically. The change from a local 3NF regulator to a local-nonlocal 3NF regulator brings an about 7% increase in the charge radius for medium-mass nuclei. The increase was observed also in previous studies [21, 56].

#### 4.3. Charge density distributions

Nuclear charge density distribution can provide more detailed information of nuclear structure, offering an even finer test for chiral Hamiltonians [57]. Theoretically, the nuclear charge density can be calculated by folding the point-nucleon

density with the intrinsic form factor of the free nucleons expressed in terms of the Sachs and Pauli form factors, see Refs. [56, 58, 59] for details of the calculation.

In this work, we focus on the charge densities of two representative closed-shell nuclei,  $^{16}\text{O}$  and  $^{40}\text{Ca}$ , whose experimental charge densities have been well measured. The converged calculations are performed using the single-reference IMSRG with  $e_{\max} = 14$ ,  $E_{3\max} = 24$  and an optimal HO frequency of  $\hbar\Omega = 16$  MeV. In both nuclei, charge density distributions calculated using 2NF(local)+3NF(lnl) are in excellent agreements with experimental data, while the densities obtained by 2NF(local)+3NF(local) are significantly larger than data in the central region of the nuclei, as shown in Fig. 6. Experimental measurements of nuclear charge density distribution remain a frontier area of nuclear physics studies [60–62]. Theoretical calculations of density distribution based on the first principles can provide deep insights into nucleon-nucleon interactions.

#### 5. Summary

Understanding the properties of atomic nuclei from first principles represents a central challenge in nuclear physics. Within the framework of chiral effective field theory, nuclear forces are hierarchically organized, where three-nucleon forces emerge as a crucial component for accurate descriptions of nuclear structure. Despite significant progresses made, a persistent challenge remains the development of a unified chiral Hamiltonian that can simultaneously reproduce the binding energy and charge radius of the nucleus.

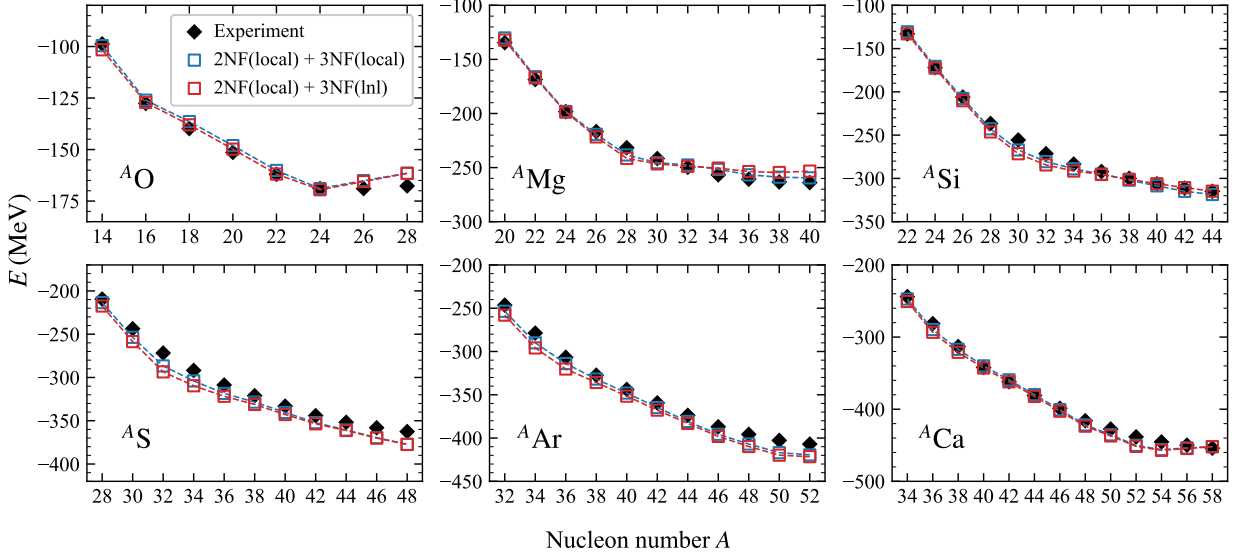


Figure 4: Ground-state energies of O, Mg, Si, S, Ar and Ca isotopes, calculated by VS-IMSRG using the new families of 2NF(local) plus 3NF(local) and 2NF(local) plus 3NF(lnl). Experimental data are taken from the 2020 atomic mass evaluation (AME2020) [48].

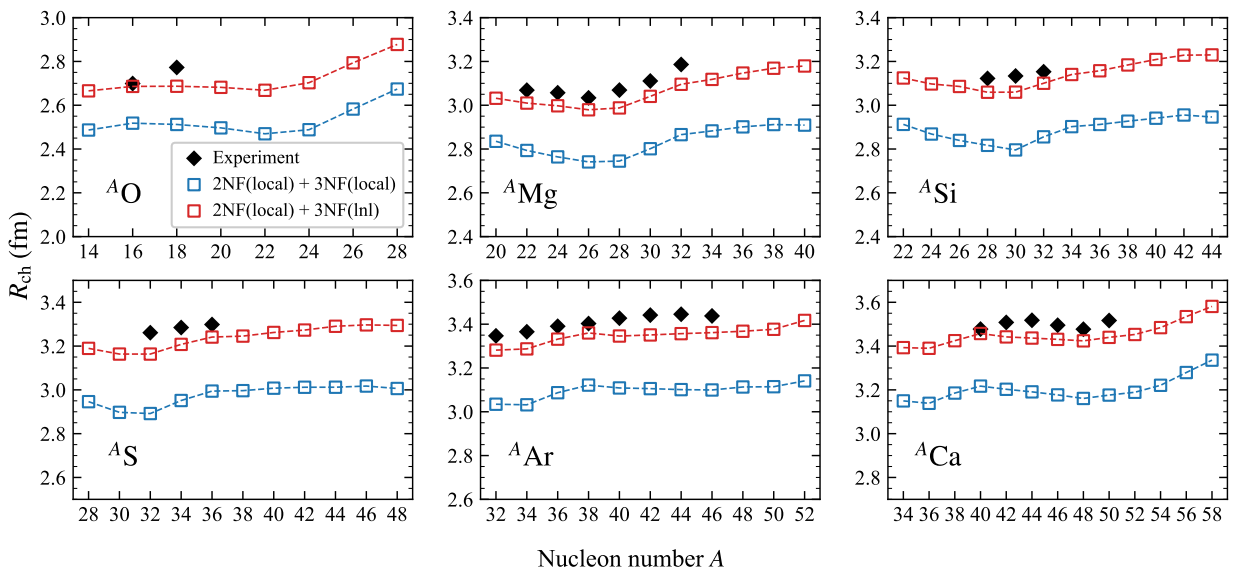


Figure 5: Similar to Fig. 4 but for charge radii. Experimental charge radii are taken from Ref. [50].

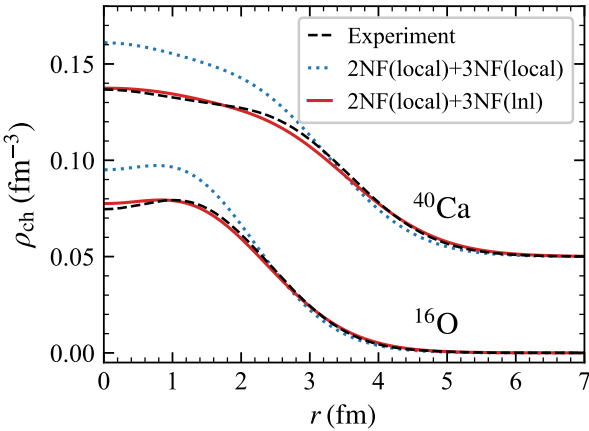


Figure 6: Charge density distributions of  $^{16}\text{O}$  and  $^{40}\text{Ca}$ , calculated with 2NF(local)+3NF(local) and 2NF(local)+3NF(lnl), compared with experimental data [63]. The density of  $^{40}\text{Ca}$  is shifted by  $0.05 \text{ fm}^{-3}$  for better readability.

In this work, we have constructed chiral three-nucleon forces at  $\text{N}^2\text{LO}$ , which form new families with the new high-quality local position-space two-nucleon interaction established by the Idaho group. The two low-energy constants,  $c_D$  and  $c_E$ , of the 3NF are constrained using the ground-state energies of  $^3\text{H}$  and  $^{16}\text{O}$ . We find that employing a local-nonlocal hybrid regularization scheme for the 3NF is particularly effective. The resulting chiral Hamiltonian is applied to many-body calculations, and provides a consistent description of experimental ground-state energy and charge radius for a wide range of nuclei, from  $^4\text{He}$  up to  $^{132}\text{Sn}$ . This work highlights that the regularization scheme of the chiral 3NF can sensitively influence the quality of many-body predictions, especially for nuclear radii. The chiral Hamiltonian developed in this work may be useful for future high-precision *ab initio* studies of nuclei.

## 6. Acknowledgements

The IMSRG calculations were performed using the `imsrg++` code [64], and chiral 3NF matrix elements were generated using the `NuHamil` code [49]. This work has been supported by the National Key R&D Program of China under Grants No. 2024YFA1610900, 2023YFA1606401, and 2023YFA1606403; the National Natural Science Foundation of China under Grants No. 12335007, 12535008, 12205340, 12347106, 12121005, and 12441506. We acknowledge the High-Performance Computing Platform of Peking University for providing computational resources.

- [1] R. Machleidt, *Few-Body Syst.* 64 (4) (2023) 77.
- [2] A. Ekström, et al., *Front. Phys.* 11.
- [3] R. Machleidt, D. Entem, *Phys. Rep.* 503 (1) (2011) 1–75.
- [4] H.-W. Hammer, S. König, U. van Kolck, *Rev. Mod. Phys.* 92 (2020) 025004.
- [5] D. R. Entem, R. Machleidt, *Phys. Rev. C* 68 (2003) 041001.
- [6] E. Epelbaum, W. Glöckle, U.-G. Meißner, *Nucl. Phys. A* 747 (2) (2005) 362–424.
- [7] D. R. Entem, R. Machleidt, Y. Nosyk, *Phys. Rev. C* 96 (2017) 024004.
- [8] E. Epelbaum, H.-W. Hammer, U.-G. Meißner, *Rev. Mod. Phys.* 81 (2009) 1773–1825.

- [9] H. Hergert, *Front. Phys.* 8.
- [10] R. Machleidt, F. Sammarruca, *Prog. Part. Nucl. Phys.* 137 (2024) 104117.
- [11] B. Hu, et al., *Nat. Phys.* 18 (10) (2022) 1196–1200.
- [12] B. C. He, S. R. Stroberg, *Phys. Rev. C* 110 (2024) 044317.
- [13] S. R. Stroberg, T. D. Morris, B. C. He, *Phys. Rev. C* 110 (2024) 044316.
- [14] A. Belley, et al., *Phys. Rev. Lett.* 132 (2024) 182502.
- [15] H. Hergert, S. Binder, A. Calci, J. Langhammer, R. Roth, *Phys. Rev. Lett.* 110 (2013) 242501.
- [16] K. Hebeler, *Phys. Rep.* 890 (2021) 1–116.
- [17] R. Machleidt, F. Sammarruca, *Eur. Phys. J. A* 56 (3) (2020) 95.
- [18] A. Ekström, et al., *Phys. Rev. Lett.* 110 (2013) 192502.
- [19] W. G. Jiang, et al., *Phys. Rev. C* 102 (2020) 054301.
- [20] T. Hüther, K. Vobig, K. Hebeler, R. Machleidt, R. Roth, *Phys. Lett. B* 808 (2020) 135651.
- [21] V. Somà, P. Navrátil, F. Raimondi, C. Barbieri, T. Duguet, *Phys. Rev. C* 101 (2020) 014318.
- [22] F. Sammarruca, R. Millerson, *Phys. Rev. C* 102 (2020) 034313.
- [23] M. C. Atkinson, W. H. Dickhoff, M. Piarulli, A. Rios, R. B. Wiringa, *Phys. Rev. C* 102 (2020) 044333.
- [24] J. Carlson, et al., *Rev. Mod. Phys.* 87 (2015) 1067–1118.
- [25] D. Lonardoni, J. Carlson, S. Gandolfi, J. E. Lynn, K. E. Schmidt, A. Schwenk, X. B. Wang, *Phys. Rev. Lett.* 120 (2018) 122502.
- [26] S. K. Saha, D. R. Entem, R. Machleidt, Y. Nosyk, *Phys. Rev. C* 107 (2023) 034002.
- [27] S. Bogner, R. Furnstahl, A. Schwenk, *Prog. Part. Nucl. Phys.* 65 (1) (2010) 94–147.
- [28] S. K. Bogner, R. J. Furnstahl, R. J. Perry, *Phys. Rev. C* 75 (2007) 061001.
- [29] A. Kuşoğlu, et al., *Phys. Rev. Lett.* 133 (2024) 072502.
- [30] P. Y. Wang, J. G. Li, S. Zhang, Q. Yuan, M. R. Xie, W. Zuo, *Phys. Rev. C* 109 (2024) 064316.
- [31] U. van Kolck, *Phys. Rev. C* 49 (1994) 2932–2941.
- [32] E. Epelbaum, et al., *Phys. Rev. C* 66 (2002) 064001.
- [33] M. Hoferichter, J. Ruiz de Elvira, B. Kubis, U.-G. Meißner, *Phys. Rev. Lett.* 115 (2015) 192301.
- [34] P. Maris, et al., *Phys. Rev. C* 103 (2021) 054001.
- [35] M. Hoferichter, J. Ruiz de Elvira, B. Kubis, U.-G. Meißner, *Phys. Rep.* 625 (2016) 1–88.
- [36] P. Navrátil, *Few-Body Syst.* 41 (3) (2007) 117–140.
- [37] P. Navrátil, V. G. Gueorguiev, J. P. Vary, W. E. Ormand, A. Nogga, *Phys. Rev. Lett.* 99 (2007) 042501.
- [38] K. Hebeler, S. K. Bogner, R. J. Furnstahl, A. Nogga, A. Schwenk, *Phys. Rev. C* 83 (2011) 031301.
- [39] S. Wesolowski, I. Svensson, A. Ekström, C. Forssén, R. J. Furnstahl, J. A. Melendez, D. R. Phillips, *Phys. Rev. C* 104 (2021) 064001.
- [40] P. Navrátil, G. P. Kamuntavičius, B. R. Barrett, *Phys. Rev. C* 61 (2000) 044001.
- [41] E. Epelbaum, H. Krebs, U.-G. Meißner, *Eur. Phys. J. A* 51 (5) (2015) 53.
- [42] S. Binder, et al., *Phys. Rev. C* 93 (2016) 044002.
- [43] S. Binder, et al., *Phys. Rev. C* 98 (2018) 014002.
- [44] K. Tsukiyama, S. K. Bogner, A. Schwenk, *Phys. Rev. Lett.* 106 (2011) 222502.
- [45] T. D. Morris, N. M. Parzuchowski, S. K. Bogner, *Phys. Rev. C* 92 (2015) 034331.
- [46] R. Roth, S. Binder, K. Vobig, A. Calci, J. Langhammer, P. Navrátil, *Phys. Rev. Lett.* 109 (2012) 052501.
- [47] S. Zhang, Y. Ma, J. Li, B. Hu, Q. Yuan, Z. Cheng, F. Xu, *Phys. Lett. B* 827 (2022) 136958.
- [48] M. Wang, W. Huang, F. Kondev, G. Audi, S. Naimi, *Chin. Phys. C* 45 (3) (2021) 030003.
- [49] T. Miyagi, *Eur. Phys. J. A* 59 (7) (2023) 150.
- [50] I. Angeli, K. Marinova, *Atomic Data and Nuclear Data Tables* 99 (1) (2013) 69–95.
- [51] P. Maris, et al., *Phys. Rev. C* 106 (2022) 064002.
- [52] S. R. Stroberg, J. D. Holt, A. Schwenk, J. Simonis, *Phys. Rev. Lett.* 126 (2021) 022501.
- [53] J. Simonis, S. R. Stroberg, K. Hebeler, J. D. Holt, A. Schwenk, *Phys. Rev. C* 96 (2017) 014303.
- [54] S. R. Stroberg, A. Calci, H. Hergert, J. D. Holt, S. K. Bogner, R. Roth, A. Schwenk, *Phys. Rev. Lett.* 118 (2017) 032502.
- [55] N. Shimizu, T. Mizusaki, Y. Utsuno, Y. Tsunoda, *Comput. Phys. Commun.* 244 (2019) 372–384.

- [56] V. Somà, C. Barbieri, T. Duguet, P. Navrátil, *Eur. Phys. J. A* 57 (4) (2021) 135.
- [57] T. Duguet, V. Somà, S. Lecluse, C. Barbieri, P. Navrátil, *Phys. Rev. C* 95 (2017) 034319.
- [58] J. W. Negele, *Phys. Rev. C* 1 (1970) 1260–1321.
- [59] P.-G. Reinhard, W. Nazarewicz, *Phys. Rev. C* 103 (2021) 054310.
- [60] T. Suda, et al., *Prog. Theor. Exp. Phys.* 2012 (1) (2012) 03C008.
- [61] K. Tsukada, et al., *Phys. Rev. Lett.* 118 (2017) 262501.
- [62] A. Antonov, et al., *Nucl. Instrum. Methods Phys. Res. Sect. A* 637 (1) (2011) 60–76.
- [63] H. De Vries, C. De Jager, C. De Vries, *Atomic Data and Nuclear Data Tables* 36 (3) (1987) 495–536.
- [64] S. R. Stroberg, <https://github.com/ragnarstroberg/imsrg> (2024).